

UC San Diego

UC San Diego Previously Published Works

Title

A single-administration therapeutic interfering particle reduces SARS-CoV-2 viral shedding and pathogenesis in hamsters

Permalink

<https://escholarship.org/uc/item/9151s6n3>

Journal

Proceedings of the National Academy of Sciences of the United States of America, 119(39)

ISSN

0027-8424

Authors

Chaturvedi, Sonali
Beutler, Nathan
Vasen, Gustavo
et al.

Publication Date

2022-09-27

DOI

10.1073/pnas.2204624119

Peer reviewed



A single-administration therapeutic interfering particle reduces SARS-CoV-2 viral shedding and pathogenesis in hamsters

Sonali Chaturvedi^{a,b,1}, Nathan Beutler^{c,1}, Gustavo Vasen^{a,b}, Michael Pablo^{a,b}, Xinyue Chen^{a,b}, Giuliana Calia^{a,b}, Lauren Buie^d, Robert Rodick^d, Davey Smith^e, Thomas Rogers^{c,e,2}, and Leor S. Weinberger^{a,b,f,g,2}

Edited by Thomas Shenk, Princeton University, Princeton, New Jersey; received March 15, 2022; accepted July 20, 2022

The high transmissibility of severe acute respiratory syndrome coronavirus 2 (SARS-CoV-2) is a primary driver of the COVID-19 pandemic. While existing interventions prevent severe disease, they exhibit mixed efficacy in preventing transmission, presumably due to their limited antiviral effects in the respiratory mucosa, whereas interventions targeting the sites of viral replication might more effectively limit respiratory virus transmission. Recently, intranasally administered RNA-based therapeutic interfering particles (TIPs) were reported to suppress SARS-CoV-2 replication, exhibit a high barrier to resistance, and prevent serious disease in hamsters. Since TIPs intrinsically target the tissues with the highest viral replication burden (i.e., respiratory tissues for SARS-CoV-2), we tested the potential of TIP intervention to reduce SARS-CoV-2 nasal shedding. Here, we report that a single, postexposure TIP dose lowers SARS-CoV-2 nasal shedding, and at 5 days postinfection, infectious virus shed is below detection limits in 4 out of 5 infected animals. Furthermore, TIPs reduce shedding of Delta variant or WA-1 from infected to uninfected hamsters. Cohoused “contact” animals exposed to infected, TIP-treated animals exhibited significantly lower viral loads, reduced inflammatory cytokines, no severe lung pathology, and shortened shedding duration compared to animals cohoused with untreated infected animals. TIPs may represent an effective countermeasure to limit SARS-CoV-2 transmission.

SARS-CoV-2 | variants | therapeutic interfering particles | lipid nanoparticle | transmission

Interrupting transmission of respiratory viruses remains a fundamental medical and public health challenge. While COVID-19 vaccines are exceptionally effective in preventing severe disease and death, accumulating data show they have mixed efficacy in preventing viral transmission (1–5), consistent with established literature that parenteral vaccines for other viruses fail to prevent mucosal virus shedding or transmission (6–8). Small-molecule antivirals, while effective in reducing viral disease pathogenesis, also appear to have inconsistent efficacy in preventing respiratory virus transmission (9, 10), including for severe acute respiratory syndrome coronavirus 2 (SARS-CoV-2) (11–13), possibly due to slow diffusion into the respiratory tract (14). Antibody-based treatments for SARS-CoV-2, which are susceptible to escape (15, 16), appear similarly unable to limit virus shedding or transmission (17), consistent with previous challenges in preventing acute respiratory infections (18). Historically, it has been proposed that interventions targeting the sites of viral replication might more effectively limit respiratory virus transmission (19, 20), but this has been challenging to demonstrate experimentally and has not been achieved in practice.

Recently, we reported that a single dose of an intranasally administered messenger RNA (mRNA)-based therapeutic interfering particle (TIP) substantially reduces SARS-CoV-2 replication, pathogenesis, and disease in Syrian golden hamsters, and exhibits a high genetic barrier to the evolution of resistance (21). Based upon the historical phenomenon of defective interfering particles (DIPs) (22–24), TIPs encode only a small, noncoding portion of the viral genome [<2 kb in the case of SARS-CoV-2 (25)] and lack self-replication but, distinct from DIPs, conditionally replicate with a reproductive number > 1 (26, 27). As obligate intracellular molecular parasites, TIPs suppress viral burst size and reduce cell-to-cell virus transmission, thereby limiting disease pathogenesis (21). The molecular mechanism of interference and conditional basic reproductive ratio (R_0) > 1 intrinsically target the TIP antiviral effect to the tissues with the highest viral replication burden (i.e., respiratory tissues for SARS-CoV-2). Therefore, we tested the potential of TIP intervention to reduce SARS-CoV-2 viral transmission (Fig. 1A).

Results and Discussion

Design of Cocaging Transmission Studies in Syrian Golden Hamsters. To test whether TIPs reduce SARS-CoV-2 transmission, we employed the Syrian golden hamster

Significance

COVID-19 vaccines are exceptionally effective in preventing severe disease and death, but they have mixed efficacy in preventing virus transmission, consistent with established literature that parenteral vaccines for other viruses fail to prevent mucosal virus shedding or transmission. Likewise, small-molecule antivirals, while effective in reducing viral disease pathogenesis, also appear to have inconsistent efficacy in preventing respiratory virus transmission, including for SARS-CoV-2. Recently, we reported the discovery of a single-administration antiviral therapeutic interfering particle (TIP) against SARS-CoV-2 that prevents severe disease in hamsters and exhibits a high genetic barrier to the evolution of resistance. Here, we report that TIP intervention also reduces SARS-CoV-2 transmission between hamsters.

Author contributions: S.C. and L.S.W. conceived and designed the study; N.B. performed hamster experiments; M.P. conceived, designed and performed modeling for the study; S.C., G.V. and G.C. designed, performed and analysed the lipid-nanoparticle studies; S.C., N.B., G.V., M.P., X.C., G.C., L.B., R.R., D.S., and T.R. designed and performed the experiments and curated the data; R.R. and L.S.W. provided reagents and resources; and S.C., G.V., M.P., R.R., D.S., and L.S.W. wrote the paper.

Competing interest statement: S.C., R.R., and L.S.W. are coinventors on a patent application filed for therapeutic interfering particles for SARS-CoV-2. L.S.W. is a scientific cofounder of VxBiosciences.

This article is a PNAS Direct Submission.

Copyright © 2022 the Author(s). Published by PNAS. This open access article is distributed under Creative Commons Attribution License 4.0 (CC BY).

¹S.C. and N.B. contributed equally to this work.

²To whom correspondence may be addressed. Email: trogers@scripps.edu or leor.weinberger@gladstone.ucsf.edu.

This article contains supporting information online at <http://www.pnas.org/lookup/suppl/doi:10.1073/pnas.2204624119/-/DCSupplemental>.

Published September 8, 2022.

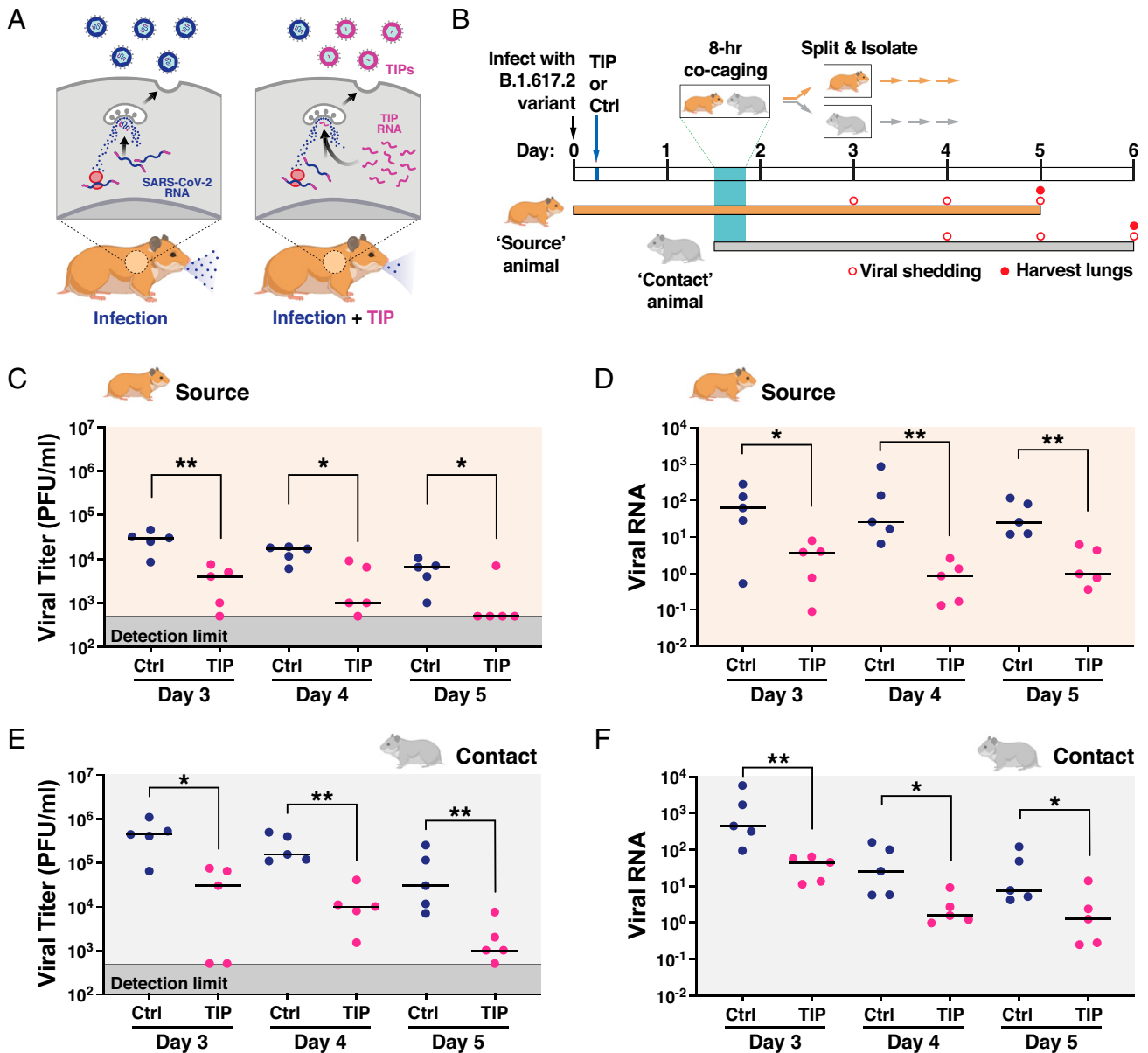


Fig. 1. TIPs reduce nasal shedding of highly pathogenic SARS-CoV-2 (B.1.617.2) in Syrian golden hamsters. (A) Schematic of putative mechanism-of-action for TIP-mediated reduction in virus transmission. (B) Schematic of experimental design. Syrian golden hamsters (source) were intranasally infected with 10^6 PFU of SARS-CoV-2 (B.1.617.2). At 6 h postinfection, TIP RNA LNPs ($n = 5$) or Ctrl RNA LNPs ($n = 5$) were intranasally administered to source animals via instillation, and hamsters were caged alone until 36 h postinfection. At 36 h, an uninfected untreated (contact) hamster was cocaged with each source hamster for 8 h. At 44 h postinfection, source and contact hamsters were separated and caged alone for the duration of the study. Nasal washes were performed at day 3 (source only), day 4 (source and contact), day 5 (source and contact), and day 6 (contact only). Source hamsters were sacrificed at day 5, and contact hamsters were sacrificed at day 6, to harvest lungs. (C) TIP treatment reduces infectious virus shedding in nasal washes. Infectious SARS-CoV-2 in nasal washes (for days 3, 4, and 5) of source animals treated with TIP ($n = 5$) or Ctrl LNPs ($n = 5$) was quantified by plaque assay. (D) TIP treatment reduces SARS-CoV-2 RNA shedding in nasal washes. Viral RNA was extracted from the nasal washes for TIP-treated ($n = 5$) or Ctrl-treated ($n = 5$) source animals at days 3, 4, and 5, and quantified by qRT-PCR for N gene. (E) Contacts of TIP-treated animals exhibit reduced infectious virus in nasal washes. Quantification of infectious SARS-CoV-2 from the nasal washes (for days 4, 5, and 6) for contacts of TIP-treated ($n = 5$) or Ctrl-treated ($n = 5$) animals was performed using plaque assay. (F) Contacts of TIP-treated animals exhibit reduced viral RNA in nasal washes. Viral RNA was extracted from the nasal washes from contacts of TIP- or Ctrl-treated animals at days 4, 5, and 6, and quantified by qRT-PCR for N gene. Medians of each arm are shown as black horizontal bars. For all panels: ** $P < 0.01$; * $P < 0.05$ from Mann-Whitney U test.

model of infection (28) based on a previously reported experimental scheme (Fig. 1B). Briefly, a group of Syrian golden hamsters were intranasally inoculated with 10^6 plaque-forming units (PFU) of SARS-CoV-2 B.1.617.2 (a.k.a., Delta variant) and designated as “source” animals. At 6 h postinfection, source animals received a single intranasal dose of either TIP RNA lipid nanoparticles (LNPs) or Ctrl RNA LNPs ($n = 5$ per group). When the source animals were near peak infectivity (36 h postinfection), each animal was cocaged for

8 h with an uninfected, untreated hamster (i.e., “contact” animal), to promote efficient (aerosol and fomite) transmission of SARS-CoV-2. At 44 h postinfection, the source and contact animals were separated into individual cages for the duration of the study. Nasal washes were then collected daily, and source and contact animals were sacrificed on days 5 and 6, respectively (i.e., ~ 5 d postinfection for each) to harvest lungs for viral titering and analysis of histopathology and inflammation.

TIPs Reduce Transmission of Highly Pathogenic SARS-CoV-2 (B.1.617.2) in Syrian Golden Hamsters. TIP-treated “source” hamsters exhibited significantly lower virus shedding in daily nasal washes, as measured by infectious virus (Fig. 1C) or viral RNA (Fig. 1D), and exhibited faster decays in nasal viral loads. Strikingly, infectious virus shed from TIP-treated animals decayed to below the limit of detection (LOD) by day 5 postinfection in four out of five animals, whereas all Ctrl-treated source animals shed high levels of virus up to day 5 (*SI Appendix, Fig. S1*). Similar reductions in nasal virus shedding were also observed for contacts of TIP- vs. Ctrl-treated animals (Fig. 1E and F).

In both source and contact animals, lungs were harvested at 5 and 6 day postinfection (Fig. 2A), and virus titer quantification was performed. TIP treatment reduced infectious SARS-CoV-2 viral load in the lungs by >3-Logs (Fig. 2B), and reduced SARS-CoV-2 RNA levels by >2-Logs (Fig. 2C). Consistent with previous reports (28, 29), contact hamsters exhibited higher viral burden than source hamsters, possibly due to the mode of inoculation—the comparatively extended 8-h aerosol plus fomite exposure—resulting in a higher viral inoculum and/or delayed viral dynamics in the contact animals.

TIP-Mediated Reduction in SARS-CoV-2 Transmission Reduces Disease Pathogenicity in Both Source and Contact Animals. Analysis of inflammatory gene expression in animal lungs showed significant reductions in inflammation in TIP-treated source animals, consistent with our previous findings (21), and significant reductions in inflammation in the contacts of TIP-treated animals (Fig. 3A). Histopathological analysis also showed substantial improvement in lung disease of TIP-treated animals, also consistent with previous data (21), as well as substantial improvement in lung disease of the contacts of TIP-treated animals (Fig. 3B and C and *SI Appendix, Fig. S2*). Since host inflammation and lung damage reflect time-integrated viral burden—whereas viral load measurements are a temporal snapshot—these inflammatory and histopathological data support the hypothesis that TIP intervention reduces viral

shedding and transmission of SARS-CoV-2, and do not support the alternate hypothesis that viral load in source animals peaked at a time not captured by the nasal wash collection schedule. Moreover, the increased viral load in the contact animals indicates that pathogenesis was not simply delayed in the contact animals compared to the source animals. Overall, the data indicate that a single intranasal dose of TIP LNPs reduces shedding and transmission of SARS-CoV-2, thus conferring protection to contact animals.

To test a second alternate hypothesis that TIPs might be mobilizing from source animals to therapeutically interfere and lower viral load within the contact animal, we used qRT-PCR to assay TIP RNA in contact animals and found no evidence of TIP transmission (*SI Appendix, Fig. S3*). These data are consistent with our previous model analysis (21) predicting that, while cell-to-cell transmission is efficient in the case of SARS-CoV-2, between-host TIP transmission faces several bottlenecks resulting in an $R_0 \ll 1$.

TIP-Mediated Transmission Reduction Is Robust across SARS-CoV-2 Strains. To verify that these transmission results were not limited to the Delta variant (B.1.617.2), we also conducted an analogous hamster transmission experiment, with the same TIP RNA, using the archival SARS-CoV-2 WA-1 strain, and observed qualitatively similar results (*SI Appendix, Fig. S4*), indicating that TIP treatment reduces viral shedding, pathogenesis, and transmission across multiple viral strains.

Viral Dynamics Models Reveal TIP-Mediated Reductions in Viral Shedding in Contact Animals. Next, to determine whether contacts of TIP-treated animals also showed reduced viral shedding, we extended an established mathematical model of viral dynamics (30) to include TIPs and then forecast the duration of infectious virus shedding from contact animal nasal wash data. Since we observed no evidence of transmission of TIPs, the viral dynamics in the contact animal were modeled without any TIPs (Fig. 4A). The model was first benchmarked against data from each individual source animal (Fig. 4B), and

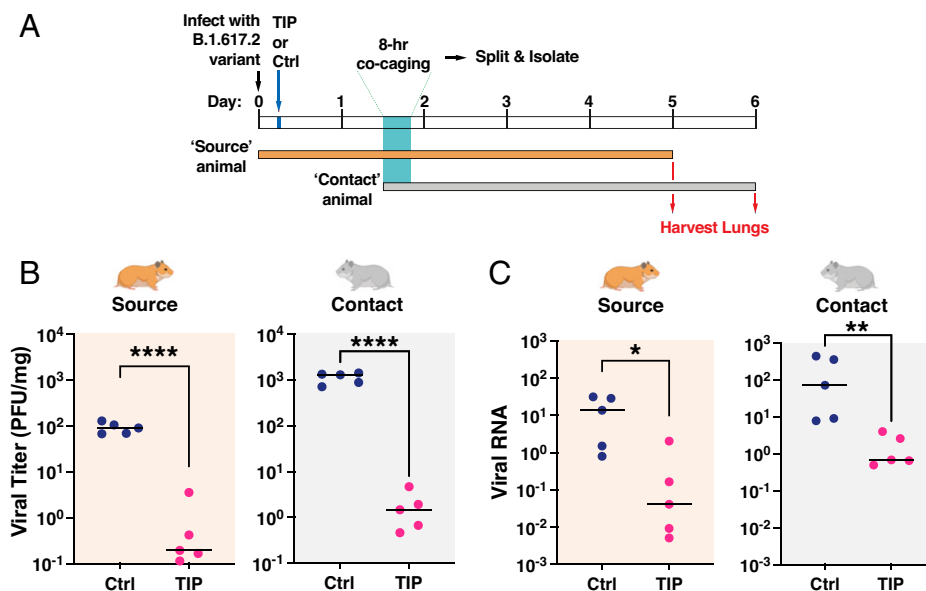


Fig. 2. TIPs reduce transmission of SARS-CoV-2 (B.1.617.2) in the lungs of Syrian golden hamsters. (A) Schematic of experimental design. (B) TIP treatment reduces infectious viral load in lungs of source hamsters and their contacts. Quantification of infectious SARS-CoV-2 in lungs of source and contact animals ($n = 5$ for all arms) as analyzed by plaque assay. (C) TIP treatment reduces viral RNA in lungs of source hamsters and their contacts. Total RNA in lungs was harvested from source and contact animals, quantified by qRT-PCR using primers specific for N gene of SARS-CoV-2 and normalized to beta-actin. Medians of each arm are shown as black horizontal bars. For all panels: **** $P < 0.0001$, *** $P < 0.01$; * $P < 0.05$ from Mann-Whitney U test.

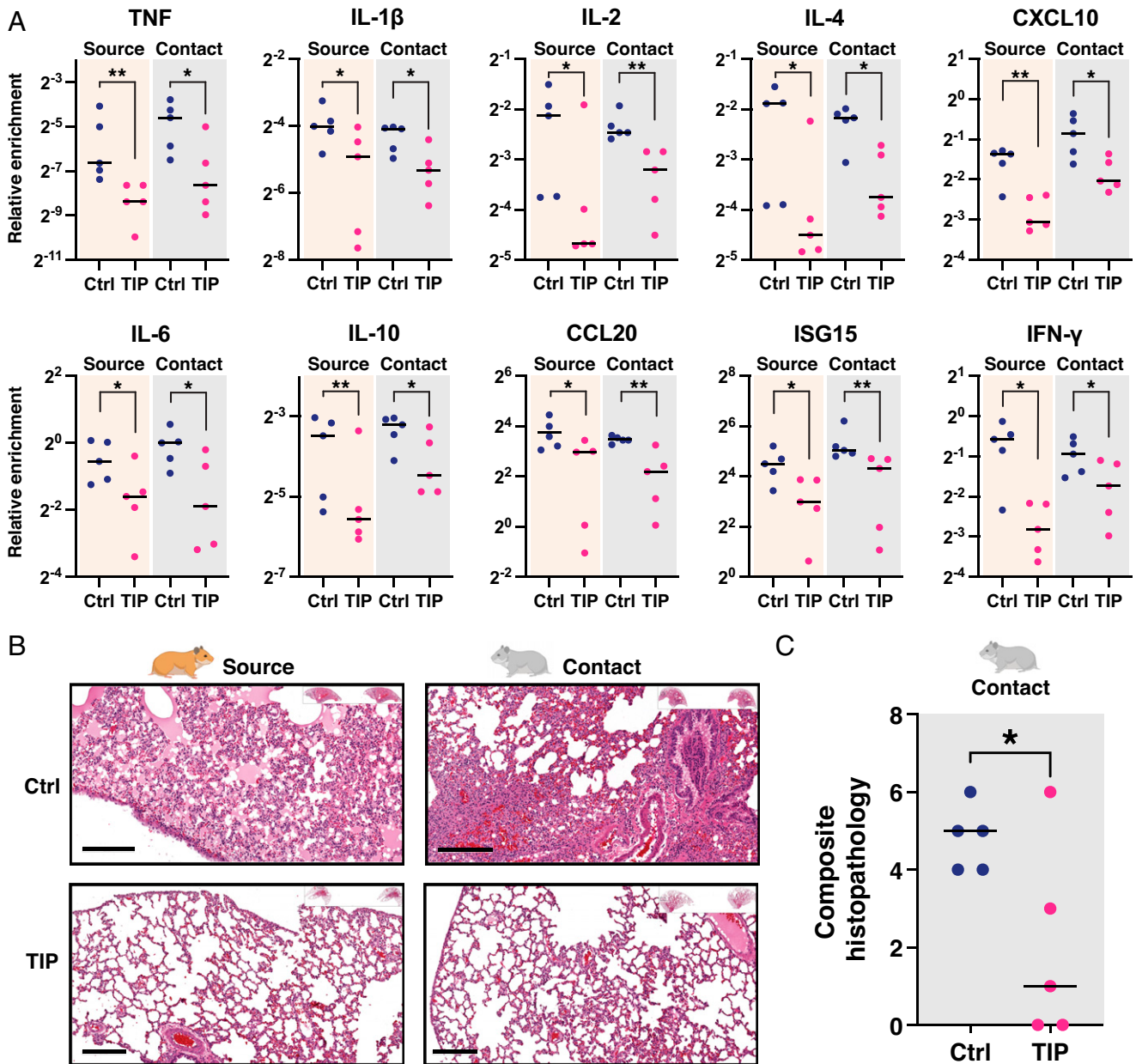


Fig. 3. TIP-mediated reduction in SARS-CoV-2 transmission reduces disease pathogenicity in both source and contact animals. (A) The qRT-PCR expression analysis for proinflammatory and interferon-stimulated genes in hamster lungs. Lungs were harvested from TIP-treated ($n = 5$) or Ctrl-treated ($n = 5$) source animals (at day 5) and their respective contact hamsters (at day 6), homogenized, and analyzed by qRT-PCR for proinflammatory cytokines and interferon-stimulated genes using respective primers and normalized to beta-actin. ** $P < 0.01$; * $P < 0.05$ from Mann-Whitney U test. (B) H&E staining of representative lung sections of TIP- and Ctrl-treated source animals and their contacts. (Scale bars, 200 μm .) (C) Histopathological scoring of lung sections for the prevalence of pulmonary infiltrates, edema, macrophages, and septum widening, resulting in a composite histopathological score ranging from a minimum of zero (indicating the absence of visual indications of pathogenicity in all scoring dimensions) to a maximum of eight (indicating end-stage pathogenesis evidenced by overwhelming infiltrates, and/or edema, macrophage, and septum widening). Medians of each arm are shown as black horizontal bars. * $P < 0.05$ from Student's t test.

it estimated that TIP-treated source animals stopped shedding 2 day faster than Ctrl-treated animals (Fig. 4D), in agreement with our experimental data (Fig. 1C and *SI Appendix*, Fig. S1). The model also indicated that TIP treatment in source animals generated a ~ 1 -Log reduction in the peak level of virus shed and in the total amount of virus shed during cohousing (Fig. 4E and F). Next, changes in contact animal shedding were estimated by fitting the now-benchmarked model to the nasal wash viral titer data from each contact hamster (Fig. 4C). The model indicated that contacts of TIP-treated animals stop shedding 2 day faster than the contacts of Ctrl-treated animals (Fig. 4G). The contacts of TIP-treated

animals also exhibit a ~ 1 -Log reduction in peak shedding compared to the contacts of Ctrl-treated animals (Fig. 4H). Collectively, this analysis suggests that postexposure TIP treatment of infected hamsters lowers transmission by reducing both the level and duration of virus shed in both source and contact animals.

Overall, these data provide proof of concept that a single-administration, postexposure intervention using mRNA-based TIP LNPs reduces the amount and duration of SARS-CoV-2 virus shedding. The data indicate that TIPs are effective against diverse archival variants (i.e., WA-1) as well as more-recent highly pathogenic variants of concern (e.g., Delta variant).

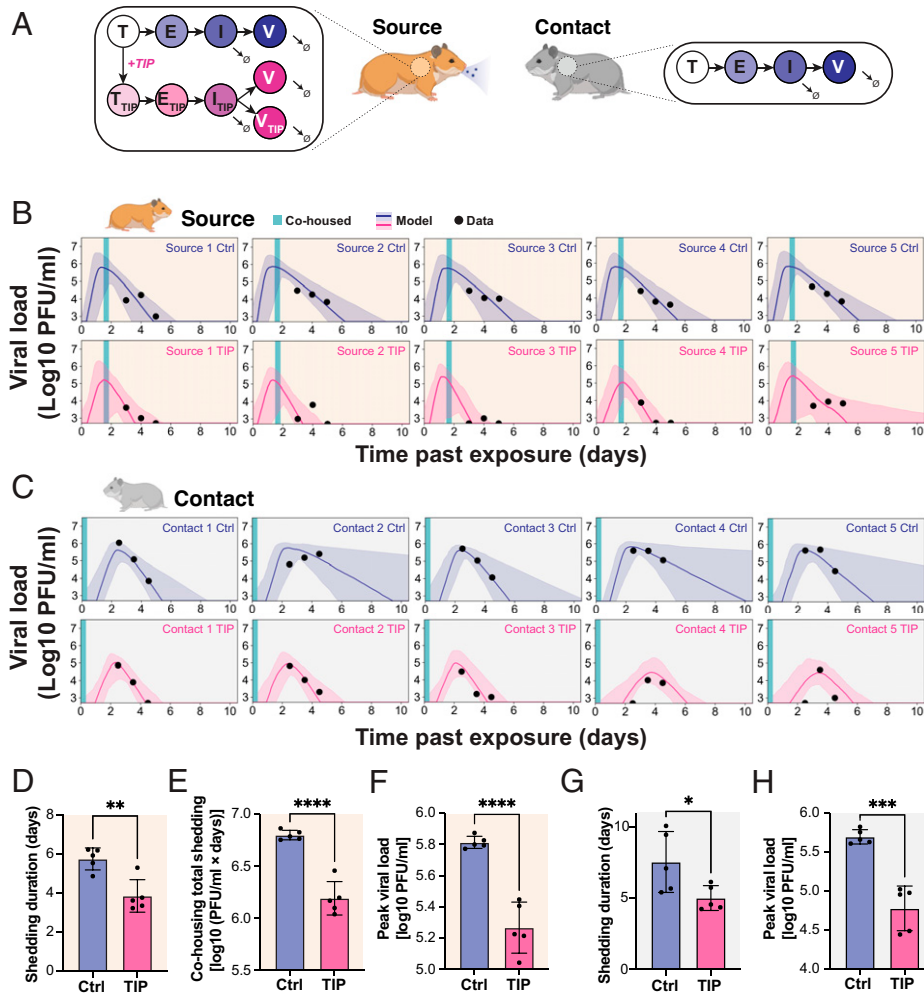


Fig. 4. Viral dynamics models reveal TIP-mediated reductions in viral shedding in contact animals. (A) Schematic of in silico model for SARS-CoV-2 dynamics in source and contact hamsters. (B) Viral dynamics models fit to nasal wash plaque assay data from source hamsters. A 95% credible interval surrounding a median prediction line is shown. The abscissa uses the time past exposure, which, for source hamsters, begins at $t = 0$ h postinfection. (C) Viral dynamics models fit to nasal wash plaque assay data from contact hamsters. A 95% credible interval surrounding a median prediction line is shown. The abscissa uses the time past exposure, which, for contact hamsters begins at $t = 36$ h postinfection of source hamsters. (D) Model inference shows that TIP reduces the duration of viral shedding in source hamsters, defined as the time until the simulated viral load dropped below the experimental LOD. (E) Model inference shows that TIP reduces the total viral shedding in source hamsters during the cohousing period, defined as the integral of the simulated viral load during cohousing. (F) Model inference shows that TIP reduces the peak viral shedding in source hamsters. (G) Model inference shows that contacts of TIP-treated animals exhibit reduced duration of viral shedding. (H) Model inference shows that contacts of TIP-treated animals exhibit reduced peak viral load. For panels D–H, each dot represents a model fit to the time course of an individual hamster; TIP ($n = 5$), Ctrl ($n = 5$); **** $P < 0.0001$; *** $P < 0.001$; ** $P < 0.01$; * $P < 0.05$ from Student's t test.

Our study has several limitations. First and foremost, the intervention was unable to fully eliminate virus transmission from source animals, since contact animals did become infected (i.e., TIP intervention did not generate transmission “sterilization”). However, as noted, similar experimental designs (9–14, 17) were employed for other antiviral interventions and failed to generate any reduction in virus transmission in hamsters. It is also possible that our experimental design of 8 h of cohousing, allowing both aerosol and fomite transmission, resulted in highly efficient, super-physiological transmission that is not reflective of what might occur between humans.

Recently, a pre-exposure prophylaxis intervention for an oral antiviral protease inhibitor was reported to inhibit transmission between hamsters (31), albeit with a substantially lower virus inoculation of 10^4 PFU than used in this study (10^6 PFU in this study) and a reduced study duration (3 day to 4 day duration vs. 5 day to 6 day duration in this study). Regardless, it is possible that pre-exposure TIP prophylaxis may similarly result in more effective transmission reduction, given our previous results (21).

Notably, translating these results to humans will require further study, given the significant physiological differences between primates and rodents (e.g., in nasal turbinate architecture and the rate of disease progression). The disease course in SARS-CoV-2 infected hamsters is highly accelerated compared to humans, such that 6 h to 12 h postinfection corresponds to ~1.25 day to 3.5 day in humans. Specifically, hamsters typically clear infectious virus (not RNA) by day 4 after peak load (28), whereas humans appear infectious 20 day to 30 day post peak load (32–34). Consequently, there appears to be roughly a 5x to 8x accelerated disease course in hamsters compared to humans. This timing may be comparable to that used for other SARS-CoV-2 antivirals that show therapeutic efficacy if administered within the first few days after onset of symptoms.

The computational models we employed also face the common limitations of such models, and the predictions will require further testing of transmission to secondary and tertiary contacts. However, the results of such secondary/tertiary transmission studies will be highly sensitive to experimental design,

and will require extensive testing of alternate timing and duration of the cohousing scenarios. Whereas the current TIPs do not appear to efficiently transmit between hosts, due to transmission bottlenecks, models predict (26, 27) that TIPs could either be engineered to transmit and thus improve population-level efficacy of the intervention or be engineered to further prevent host transmission as a safety measure. Broadly, the data herein validate the concept that antiviral interventions which specifically target the site of viral replication may effectively reduce respiratory virus transmission.

Materials and Methods

Virus and Cell Culture Conditions. SARS-CoV-2 isolate (USA-WA1/2020) and SARS-CoV-2 variant (B.1.617.2) were obtained from BEI Resources. Vero E6 cells were used to prepare viral stocks in Dulbecco's modified Eagle's medium (DMEM) supplemented with 10% fetal bovine serum (FBS) and 1% penicillin and streptomycin (P/S). All live virus experiments were performed at Gladstone Institutes in a Biosafety Level 3 (BSL3) containment facility, or at the Scripps Research Institute in an Animal BSL3 containment facility. All live virus experiments at Gladstone were performed under an approved Biosafety Use Authorization from University of California San Francisco (UCSF) in compliance with institutional guidelines and procedures. All live virus experiments at Scripps were performed under an approved Biosafety Use Authorization from University of California San Diego in compliance with institutional guidelines and procedures. Vero E6 cells (ATCC, CRL-1586) were maintained in DMEM supplemented with 1% P/S and 10% FBS and cultured under 5% CO₂ in a humidified incubator at 37 °C.

In Vitro Transcription of RNA. RNA was in vitro transcribed from 1 µg of agarose gel-purified band corresponding to the intended size using HiScribe T7 high yield RNA synthesis kit (cat#E2040S, New England Biolabs Inc.) followed by adding a 5' cap using the Vaccina Capping System (cat#M2080S, New England Biolabs Inc.) and a poly-A tail using *Escherichia coli* Poly(A) polymerase (cat#M0276S, New England Biolabs Inc.). Transcribed RNA was purified using phenol-chloroform extraction, followed by ethanol precipitation, and resuspended in nuclease-free water.

LNP Formulation and Characterization. RNA was packaged into LNPs using a NanoAssemblr microfluidic system (Precision Nanosystems) according to the manufacturer's instruction. Briefly, LNP formulations were prepared by injecting 12.5 mM lipid solution and 0.173 µg/µL RNA in formulation buffer at a flow rate of 12 mL/min. LNP suspension was immediately diluted in phosphate-buffered saline (PBS) (cat#21-040-CM, Corning) followed by reconcentration of formulation by centrifuging at 2,000 × *g* in Amicon filters (30,000 MWCO, Amicon Ultra-15 Centrifugal filter unit cat# Z717185, Millipore Sigma). The LNP suspension was filtered through a 0.22µm syringe filter, and LNPs were stored at 4 °C until use. Free and total RNA concentrations were determined by Ribogreen assay (Quant-iT RiboGreen RNA, cat# R11490, Invitrogen). LNPs were lysed for 10 min at 37 °C in 1% Triton X-100 to obtain total RNA concentration. Encapsulated RNA was calculated as (([total RNA] - [free RNA])/[total RNA] × 100). The size of LNPs was characterized by dynamic light scattering in a DynaPro NanoStar Instrument (Wyatt Technology) and analyzed with Dynamics 8.0 software (Wyatt Technology). The LNPs were used within 5 days of making them.

Transmission Experiment. All Syrian golden hamsters (Hamster/Golden Syrian Hamster/Male/6 to 8 weeks old/Charles River/Strain Code 049) experiments were approved by the Scripps Research Institute Institutional Animal Care and Use Committee/Protocol 20-0003, and were carried out in accordance with recommendations. The 8-week-old Syrian golden hamsters were intranasally infected with 10⁶ PFU of SARS-CoV-2 (USA-WA1/2020) or SARS-CoV-2 variant (B.1.617.2) in 100 µL of DMEM, as described (35). At 6 h postinfection (for B.1.617.2 infected hamsters); 12 h postinfection (for USA-WA1/2020), hamsters were intranasally dosed with 100 µL of LNP solution from either TIP RNA (*n* = 5) or Ctrl RNA (*n* = 5). At 36 h postinfection, the source animals were cocaged with naïve animals (contact animals) for 8 h; then all animals were caged individually starting 44 h postinfection. Nasal washes were collected for source animals on

days 3, 4, and 5 and for contact animals on days 4, 5, and 6, followed by harvesting of lungs at day 5 for source and day 6 for contact animals.

Plaque Assay. Infectious virus was quantified by plaque assay on Vero E6 cells. Briefly, Vero E6 cells were plated as a confluent monolayer in 12-well plates 24 h before performing the plaque assay. On the day of plaque assay, media was aspirated, followed by washing cells with 2 mL of PBS. Virus dilution was performed in modified DMEM media (DMEM, 2% FBS, L-glut, P/S), followed by adding 250 µL of diluted virus to the confluent monolayer. The plates were incubated at 37 °C for 1 h with gentle rocking every 15 min. After 1 h of incubation, 2 mL of overlay media (1.2% Avicel in 1× MEM) was added to each well and transferred to an incubator. At 3 day postinfection, overlay media was gently aspirated, and the monolayer was washed with PBS, fixed with 10% formalin for 1 h, and stained with 0.1% crystal violet, followed by washing with cell culture-grade water. The plaques were enumerated, and virus titer was calculated to PFU per milliliter or milligram of tissue.

RNA Extraction and qRT-PCR Titering of Virus. At indicated time points, lung homogenate or nasal washes were lysed in TRIzol LS (cat#10296010, Invitrogen), using 0.75 mL of TRIzol LS for 0.25-mL sample volume. RNA was extracted using the Direct-zol RNA extraction kit (cat#R2070T, Zymo Research Inc.). RNA was DNase treated using RNase-free Dnase I (cat#ENO521, ThermoFisher Scientific). One microgram of RNA was reverse transcribed using SuperScript II Reverse Transcriptase with oligo d(T) primers (cat#12574026, ThermoFisher Scientific), and complementary DNA was analyzed by qRT-PCR analysis using SYBR green PCR master mix (cat#4309155, ThermoFisher Scientific) with sequence-specific primers. All the lung homogenate samples were normalized to beta-actin (SI Appendix, Table S1).

Histopathology. Formalin-fixed lung from each animal was processed and paraffin embedded, and tissue sections were stained with hematoxylin and eosin (H&E) as described (36). Samples were imaged and analyzed using the Leica Aperio ImageScope software. Histopathological scoring was performed based on established algorithms (37–39) to devise a continuous numerical scale for determining the degree of pathogenicity in lung specimens for correlation with viral titer (PFU and qPCR) and inflammatory expression data. Specifically, the multiparametric quantitative scoring system analyzed a blinded histology image that considered the prevalence of pulmonary infiltrates, edema, macrophages, and septum widening, resulting in a composite histopathological score ranging from a minimum of zero (indicating the absence of visual indications of pathogenicity in all scoring dimensions) to a maximum of eight (indicating end-stage pathogenesis evidenced by overwhelming infiltrates, and/or edema, macrophage, and septum widening). Lungs with a score of three or lower were considered to be healthy lungs, with predominantly unobstructed alveolar capacity (37–39).

Mathematical Modeling and Model Inference. The following system of ordinary differential equations was used to model viral dynamics within individual hamsters:

$$\frac{dT}{dt} = -\beta VT - \beta V_{TIP} T$$

$$\frac{dE}{dt} = +\beta VT - kE$$

$$\frac{dI}{dt} = +kE - \delta I$$

$$\frac{dV}{dt} = \pi I - cV + \psi \pi I_{TIP}$$

$$\frac{dT_{TIP}}{dt} = -\beta V T_{TIP} + \beta V_{TIP} T$$

$$\frac{dE_{TIP}}{dt} = +\beta V T_{TIP} - kE_{TIP}$$

$$\frac{dI_{TIP}}{dt} = +kE_{TIP} - \delta I_{TIP}$$

$$\frac{dV_{TIP}}{dt} = -cV_{TIP} + \rho \pi I_{TIP},$$

where *T* corresponds to naïve target cells, *E* corresponds to nonproductively infected cells, *I* corresponds to productively infected cells, and *V* corresponds to

SARS-CoV-2 viral load. These discrete states and their transitions are typical of viral dynamics models (30, 40, 41). We extend this model to have parallel TIP-carrying states: T_{TIP} corresponds to TIP-carrying target cells, E_{TIP} corresponds to TIP-carrying nonproductively infected cells, I_{TIP} corresponds to TIP-carrying productively infected cells, and V_{TIP} corresponds to TIP load. The parameter β is the infectivity, k is the rate of progression to productive infection, δ is the death rate of infected cells, c is the TIP and virus clearance rate, π is the virus production rate, ρ is the TIP production rate relative to SARS-CoV-2, and ψ is the SARS-CoV-2 production rate in I_{TIP} cells relative to untreated infected cells. We assume $\rho = 1.5$ and $\psi = 0.02$ based on prior measurements (21).

For Ctrl-treated sources and contacts, all the TIP-related state variables were set to zero. For TIP-treated sources, a nonzero $V_{TIP,i}$ was defined, representing the amount of TIP administered at $t = 8$ h. For contacts of TIP-treated animals, we assumed no TIP transmission, by setting all the TIP-related state variables to zero. We assumed there are 10^7 target cells (T) as a rough estimate of the number of SARS-CoV-2 susceptible cells in the hamster respiratory system (42).

A two-stage approach was used to fit the model to the nasal wash plaque assay data. First, initial parameter estimates were generated by fitting only control-treated source hamsters within a nonlinear mixed-effects model framework (Monolix version 2020R1: Lixoft SAS, 2020). At this stage, the rate of progression to productive infection, k , was fixed to 4 d^{-1} , and the virion burst size π was fit to $10 \text{ PFU} \cdot \text{mL}^{-1} \cdot \text{d}^{-1}$ under the assumption that the single-cell replication kinetics would not change substantially between hamsters. By fitting the control source dataset, we obtained representative parameter estimates for the population of control-treated source hamsters. For the next stage, these estimates were used to set priors for the Delayed Rejection Adaptive Metropolis variation of Markov chain Monte Carlo (DRAM-MCMC) (43, 44). DRAM-MCMC was used to fit the nasal wash plaque assay data for each hamster separately, obtaining posterior distributions of model parameters and predicted viral dynamics. Gaussian priors were used on β , δ , c , and $\log_{10}(V_i)$, and for TIP-treated source hamsters, $\log_{10}(V_{TIP,i})$. The viral inoculum and TIP dosage were sampled in logarithmic space. We assumed the prior was strongly informative for β ($\mu_\beta = 0.000031$, $\sigma_\beta = 0.00001$) but uninformative for δ ($\mu_\delta = 1.87$, $\sigma_\delta = \infty$), c ($\mu_c = 1.87$, $\sigma_c = \infty$), $\log_{10}(V_i)$ ($\mu_{\log_{10}(V_i)} = 6$, $\sigma_{\log_{10}(V_i)} = \infty$), and $\log_{10}(V_{TIP,i})$ ($\mu_{\log_{10}(V_{TIP,i})} = 6$, $\sigma_{\log_{10}(V_{TIP,i})} = \infty$). Narrowing the priors did not influence the quality of model fits. The sampling range for parameters was $\beta \in [0, 1]$, $\delta \in [0, 100]$, $c \in [0, 100]$, $\log_{10}(V_i) \in [1, 7]$, $\log_{10}(V_{TIP,i}) \in [1, 7]$.

The following error function was minimized:

$$Error = \sum (y - \hat{y})^2 + f_{peak}(\hat{t}_{peak}; t_{peak})$$

$$f_{peak}(\hat{t}_{peak}; t_{peak}) = \begin{cases} 0, & \text{if } \hat{t}_{peak} \text{ is within } t_{peak} \pm 1 \text{ day} \\ (t_{peak} - \hat{t}_{peak})^2, & \text{otherwise} \end{cases}$$

1. D. W. Eyre *et al.*, Effect of Covid-19 vaccination on transmission of alpha and delta variants. *N. Engl. J. Med.* **386**, 744–756 (2022).
2. C. M. Brown *et al.*, Outbreak of SARS-CoV-2 infections, including COVID-19 vaccine breakthrough infections, associated with large public gatherings - Barnstable County, Massachusetts, July 2021. *MMWR Morb. Mortal. Wkly. Rep.* **70**, 1059–1062 (2021).
3. S. Hayek *et al.*, Indirect protection of children from SARS-CoV-2 infection through parental vaccination. *Science* **375**, 1155–1159 (2022).
4. O. Prunas *et al.*, Vaccination with BNT162b2 reduces transmission of SARS-CoV-2 to household contacts in Israel. *Science* **375**, 1151–1154 (2022).
5. A. Singanayagam *et al.*, ATACCC Study Investigators, Community transmission and viral load kinetics of the SARS-CoV-2 delta (B.1.617.2) variant in vaccinated and unvaccinated individuals in the UK: A prospective, longitudinal, cohort study. *Lancet Infect. Dis.* **22**, 183–195 (2022).
6. T. R. Hird, N. C. Grassly, Systematic review of mucosal immunity induced by oral and inactivated poliovirus vaccines against virus shedding following oral poliovirus challenge. *PLoS Pathog.* **8**, e1002599 (2012).
7. A. C. Lowen *et al.*, Blocking interhost transmission of influenza virus by vaccination in the guinea pig model. *J. Virol.* **83**, 2803–2818 (2009).
8. J. L. Schulman, Experimental transmission of influenza virus infection in mice. 3. Differing effects of immunity induced by infection and by inactivated influenza virus vaccine on transmission of infection. *J. Exp. Med.* **125**, 467–478 (1967).
9. D. H. Cheung *et al.*, Association of oseltamivir treatment with virus shedding, illness, and household transmission of influenza viruses. *J. Infect. Dis.* **212**, 391–396 (2015).
10. T. Umemura *et al.*, Efficacy of baloxavir marboxil on household transmission of influenza infection. *J. Pharm. Health Care Sci.* **6**, 21 (2020).
11. R. M. Cox, J. D. Wolf, R. K. Plemper, Therapeutically administered ribonucleoside analogue MK-4482/EIDD-2801 blocks SARS-CoV-2 transmission in ferrets. *Nat. Microbiol.* **6**, 11–18 (2021).
12. K. Rosenke *et al.*, Orally delivered MK-4482 inhibits SARS-CoV-2 replication in the Syrian hamster model. *Nat. Commun.* **12**, 2295 (2021).

where $\sum (y - \hat{y})^2$ is the sum of squared errors from the data, and $f_{peak}(\hat{t}_{peak}; t_{peak})$ is a penalty function constraining the predicted timing of the peak viral load (\hat{t}_{peak}) based on prior infection time course studies (28). Specifically, for source hamsters, we assume $t_{peak} = 2$, and, for contact hamsters, we assume $t_{peak} = 3$. All simulated data points below the LOD (500 PFU/mL) were left-censored prior to calculating errors or prediction intervals. We ran 10,000 steps of DRAM-MCMC using a prior for the error variance defined by $S_0^2 = 0.1$ and $N_0 = 20$, which was empirically found to have a sufficient rejection frequency ($\sim 40\%$) for sampling. The first 1,000 steps of DRAM-MCMC were discarded as burn-in, and 1,000 samples were drawn from the remaining chain to generate the posterior prediction intervals. The errors converged within this time frame (SI Appendix, Fig. S5A) despite substantial uncertainty in individual parameters (SI Appendix, Fig. S5B). The median of the prediction intervals (dark lines within shaded regions in Fig. 4 B and C) were used to infer clearance time, integrated viral shedding, and peak viral shedding.

Statistical Analysis. Statistical differences were determined by using a two-tailed unpaired Mann-Whitney U test, unless otherwise mentioned (GraphPad Prism). A P value less than 0.05 was considered statistically significant: * <0.05 , ** <0.01 , *** <0.001 , **** <0.0001 , ns: not significant.

Data, Materials, and Software Availability. All unique reagents generated in this study are available from the Lead Contact with a completed Materials Transfer agreement. All data, code, and materials used in the analysis have been deposited in Zenodo (<https://zenodo.org/record/6762604>) (45). All study data are included in the article and/or supporting information.

ACKNOWLEDGMENTS. We thank K. Claiborn for editing; Blaise Ndjamen and F. N. N. Pitchai for technical guidance; and the Gladstone-UCSF Center For AIDS Research (CFAR) flow-cytometry core, funded by NIH Grants P30 AI027763 and S10 RR028962 and the James B. Pendleton Trust; as well as the Gladstone Genomics and Histology Cores. This work was supported by Pamela and Edward Taft (to L.S.W.), US Army Medical Infectious Disease Research Program (Award MTEC-20-09-COVID19-064) (to L.S.W.), and NIH Awards DP1DA051144 (to L.S.W.) and R01AI169443 (to L.S.W. and R.R.).

Author affiliations: ^aGladstone/UCSF Center for Cell Circuitry, San Francisco, CA 94158; ^bGladstone Institute of Virology, Gladstone Institutes, San Francisco, CA 94158; ^cDepartment of Immunology and Microbiology, The Scripps Research Institute, La Jolla, CA 92037; ^dVxBiosciences Inc., Berkeley, CA 94707; ^eDivision of Infectious Diseases, Department of Medicine, University of California San Diego, La Jolla, CA 92121; ^fDepartment of Biochemistry and Biophysics, University of California, San Francisco, CA 94158; and ^gDepartment of Pharmaceutical Chemistry, University of California, San Francisco, CA 94158

13. J. A. Belser *et al.*, Ferrets as models for influenza virus transmission studies and pandemic risk assessments. *Emerg. Infect. Dis.* **24**, 965–971 (2018).
14. G. He, J. Massarella, P. Ward, Clinical pharmacokinetics of the prodrug oseltamivir and its active metabolite Ro 64-0802. *Clin. Pharmacokinet.* **37**, 471–484 (1999).
15. D. Planas *et al.*, Reduced sensitivity of SARS-CoV-2 variant Delta to antibody neutralization. *Nature* **596**, 276–280 (2021).
16. S. Cele *et al.*, Network for Genomic Surveillance in South Africa; COMMIT-KZN Team, Escape of SARS-CoV-2 501Y.V2 from neutralization by convalescent plasma. *Nature* **593**, 142–146 (2021).
17. S. Horiuchi *et al.*, Immune memory from SARS-CoV-2 infection in hamsters provides variant-independent protection but still allows virus transmission. *Sci. Immunol.* **6**, eabm3131 (2021).
18. S. K. Lai, M. D. McSweeney, R. J. Pickles, Learning from past failures: Challenges with monoclonal antibody therapies for COVID-19. *J. Control. Release* **329**, 87–95 (2021).
19. L. Zeitlin, R. A. Cone, K. J. Whaley, Using monoclonal antibodies to prevent mucosal transmission of epidemic infectious diseases. *Emerg. Infect. Dis.* **5**, 54–64 (1999).
20. S. Afkhami *et al.*, Respiratory mucosal delivery of next-generation COVID-19 vaccine provides robust protection against both ancestral and variant strains of SARS-CoV-2. *Cell* **185**, 896–915.e19 (2022).
21. S. Chaturvedi *et al.*, Identification of a therapeutic interfering particle-A single-dose SARS-CoV-2 antiviral intervention with a high barrier to resistance. *Cell* **184**, 6022–6036.e18 (2021).
22. P. Von Magnus, Incomplete forms of influenza virus. *Adv. Virus Res.* **2**, 59–79 (1954).
23. A. S. Huang, D. Baltimore, Defective viral particles and viral disease processes. *Nature* **226**, 325–327 (1970).
24. M. Vignuzzi, C. B. López, Defective viral genomes are key drivers of the virus-host interaction. *Nat. Microbiol.* **4**, 1075–1087 (2019).
25. S. Yao, A. Narayanan, S. A. Majowicz, J. Jose, M. Archetti, A synthetic defective interfering SARS-CoV-2. *PeerJ* **9**, e11686 (2021).
26. V. T. Metzger, J. O. Lloyd-Smith, L. S. Weinberger, Autonomous targeting of infectious superspreaders using engineered transmissible therapies. *PLOS Comput. Biol.* **7**, e1002015 (2011).

27. L. S. Weinberger, D. V. Schaffer, A. P. Arkin, Theoretical design of a gene therapy to prevent AIDS but not human immunodeficiency virus type 1 infection. *J. Virol.* **77**, 10028–10036 (2003).
28. S. F. Sia *et al.*, Pathogenesis and transmission of SARS-CoV-2 in golden hamsters. *Nature* **583**, 834–838 (2020).
29. Y. J. Hou *et al.*, SARS-CoV-2 D614G variant exhibits efficient replication ex vivo and transmission in vivo. *Science* **370**, 1464–1468 (2020).
30. A. S. Perelson, Modelling viral and immune system dynamics. *Nat. Rev. Immunol.* **2**, 28–36 (2002).
31. R. Abdelnabi *et al.*, The oral protease inhibitor (PF-07321332) protects Syrian hamsters against infection with SARS-CoV-2 variants of concern. *Nat. Commun.* **13**, 719 (2022).
32. T. C. Jones *et al.*, Estimating infectiousness throughout SARS-CoV-2 infection course. *Science* **373**, eabi5273 (2021).
33. R. Wölfel *et al.*, Virological assessment of hospitalized patients with COVID-2019. *Nature* **581**, 465–469 (2020).
34. R. A. P. M. Perera *et al.*, SARS-CoV-2 virus culture and subgenomic RNA for respiratory specimens from patients with mild coronavirus disease. *Emerg. Infect. Dis.* **26**, 2701–2704 (2020).
35. T. F. Rogers *et al.*, Isolation of potent SARS-CoV-2 neutralizing antibodies and protection from disease in a small animal model. *Science* **369**, 956–963 (2020).
36. A. H. Fischer, K. A. Jacobson, J. Rose, R. Zeller, Hematoxylin and eosin staining of tissue and cell sections. *CSH Protoc.* **2008**, pdb prot4986 (2008).
37. T. Ashcroft, J. M. Simpson, V. Timbrell, Simple method of estimating severity of pulmonary fibrosis on a numerical scale. *J. Clin. Pathol.* **41**, 467–470 (1988).
38. R. Klopfeisch, Multiparametric and semiquantitative scoring systems for the evaluation of mouse model histopathology—A systematic review. *BMC Vet. Res.* **9**, 123 (2013).
39. K. N. Gibson-Corley, A. K. Olivier, D. K. Meyerholz, Principles for valid histopathologic scoring in research. *Vet. Pathol.* **50**, 1007–1015 (2013).
40. R. Ke, C. Zitzmann, D. D. Ho, R. M. Ribeiro, A. S. Perelson, In vivo kinetics of SARS-CoV-2 infection and its relationship with a person's infectiousness. *Proc. Natl. Acad. Sci. U.S.A.* **118**, e2111477118 (2021).
41. A. Goyal, D. B. Reeves, E. F. Cardozo-Ojeda, J. T. Schiffer, B. T. Mayer, Viral load and contact heterogeneity predict SARS-CoV-2 transmission and super-spreading events. *eLife* **10**, e63537 (2021).
42. A. R. Kennedy, A. Desrosiers, M. Terzaghi, J. B. Little, Morphometric and histological analysis of the lungs of Syrian golden hamsters. *J. Anat.* **125**, 527–553 (1978).
43. H. Haario, M. Laine, A. Mira, E. Saksman, DRAM: Efficient adaptive MCMC. *Stat. Comput.* **16**, 339–354 (2006).
44. P. R. Miles, pymcstat: A Python package for Bayesian inference using Delayed rejection adaptive metropolis. *J. Open Source Softw.* **4**, 1417 (2019).
45. S. Chaturvedi *et al.*, A single-administration therapeutic interfering particle reduces SARS-CoV-2 viral shedding and pathogenesis in hamsters. Zenodo. <https://zenodo.org/record/6762604>. Deposited 27 June 2022.